Energy Reports 8 (2022) 6753–6763

Contents lists available at ScienceDirect

Energy Reports

journal homepage: www.elsevier.com/locate/egyr

Research paper

Towards the "sustainable" operation at -30 °C without the expense of energy for heating on-face electronics: Intelligent heat conservation and waste heat utilization

Tianle Zhou [a,b,c,d,*], Zheng-Dong Chen [a], Shuang-Qin Chen [d,e], Feng Wang [b], Yizhi Zhuo [b], Zhiliang Zhang [b], Jianying He [b], Huaping Tan [a,d], Xiaoheng Liu [c], Xin Wang [c]

[a] School of Materials Science and Engineering, Nanjing University of Science and Technology, Nanjing 210094, China
[b] NTNU Nanomechanical Lab, Department of Structural Engineering, Norwegian University of Science and Technology, Trondheim 7491, Norway
[c] Country Key Laboratory for Soft Chemistry and Functional Materials of Ministry Education, Nanjing University of Science and Technology, Nanjing 210094, China
[d] Jiangsu Key Laboratory of Advanced Micro & Nano Materials and Technology, Nanjing University of Science and Technology, Nanjing 210094, China
[e] Herbert Gleiter Institute of Nanoscience, Nanjing University of Science and Technology, Nanjing 210094, China

ARTICLE INFO

Article history:
Received 10 February 2022
Received in revised form 26 April 2022
Accepted 10 May 2022
Available online xxxx

Keywords:
On-skin electronics
Intelligent energy conservation
Super-hygroscopic gel
Cellulose hydrogel
Skin moisture
Waste heat utilization

ABSTRACT

On-face electronics (On-faceE) are urged to sense "anytime, anywhere" for enabling human senses to globally dominate the Internet of Things. However, with the limited lifetime of batteries and the miniaturization of the On-faceE, On-faceE are confronting two challenges: sustainable operation at the temperature (T) < 0 °C and frost/ice accretion security hazard. Of note, the face and On-faceE themselves continuously generate heat and are more reliable than solar-/motion-based heat supplies. However, such self-generated heat often occurs as waste heat, lost into the environment. Here, a film pioneering the intelligent conservation and utilization of this waste self-generated heat for enabling On-faceE to work even at -30 °C for 8 h is developed, through making a versatile cellulose hydrogel and enabling the super-hygroscopic gel to capture moisture at the T < 0 °C. It creates a ΔT up to 60 °C between inside T and ambient T (-30 °C) after sealing On-faceE and, importantly, intelligently stops conserving heat when the working T > 30 °C and demonstrates outstanding heat-conserving stability and sustainability, thus solving the two challenges without the expense of energy for heating and positioning it as an energy-saving "smart" T-regulating candidate. This work could address the energy shortage and heating costs for conquering low-T limitations for globalizing On-faceE.

1. Introduction

The onset of on-skin electronics for the Internet of Things (IoT) is creating a revolution as they help in various sensor domains yet regardless of time and place, breaking the boundaries of smart cities (Kim et al., 2021; Lim et al., 2020; Zhu et al., 2021). In particular, the fusion of on-face electronics (On-faceE) and IoT holds a strong future as the face gathers the most vital sensory organ network (eyes + nose + ears).

On-faceE are urged to sense "anytime, anywhere" for enabling human senses to globally dominate the IoT; however, are facing certain limitations. The face has rich blood circulation thus self-thermoregulation functions, but On-faceE would be on strike at the temperature (T) < 0 °C (Wu et al., 2020; Ying et al., 2021). Besides, the face moisture gathered by mask (COVID-19 necessitates using masks as a routine) not only induces skin irritation but causes frost/ice accretion as encountering the low-T surface of On-faceE, seriously threatening the security of On-faceE + IoT (Wu et al., 2020; Ying et al., 2021; Shrivastav et al., 2020). In brief, with the limited lifetime of batteries and the miniaturization of the On-faceE, On-faceE are facing two challenges: sustainable operation at the T < 0 °C and frost/ice accretion security hazard.

Nowadays, "The 2030 Agenda for Sustainable Development" proposed by United Nations has been widely recognized. How to improve energy efficiency has become a key issue. Today, the heating energy demand has become a significant estimator used during the design stage of any new On-faceE, as the current reliance on batteries is unsustainable. Of note, the face and On-faceE themselves continuously generate heat and are more reliable than solar-/motion-based heat supplies (e.g., the face alone continuously emits ~20 mW cm^{-2} heat Liu et al., 2020). However, such self-generated heat often occurs as waste heat,

* Corresponding author at: School of Materials Science and Engineering, Nanjing University of Science and Technology, Nanjing 210094, China.
E-mail address: ztltianle999@hotmail.com (T. Zhou).

https://doi.org/10.1016/j.egyr.2022.05.024

lost into the environment. Despite the booming of thermoelectric studies in terms of raising energy efficiency (Zhou et al., 2019; Nozariasbmarz et al., 2020), it is still a challenge to design a system converting enough energy to sustainably heating On-faceE (Thomas, 2020). Noteworthily, by now, few works have been done with a broader horizon — "conserving instead of converting" the self-generated heat, which has more substantial benefits for energy efficiency.

Heat is lost in three ways: conduction, convection, and radiation. A heat-insulated, anti-freezing, breathable film with the characteristics of ultra-stretchability can conformally seal the complex contour of On-faceE and time-dynamic curvilinear skin to prevent the heat conduction and part of heat convection under the premise of guaranteeing adequate breathability. However, the "On-faceE"-oriented fabrication of such a film featuring the combined ultra-stretchability, excellent anti-freezing, and adequate breathability is still an open issue.

Besides conduction and convection, mid-infrared (IR) radiation plays a dominating role in heat loss (e.g., it occupies >50% of the heat loss of the face) (Peng and Cui, 2020; Moghimi et al., 2018). Of note, the emerging super-hygroscopic gels are propelling a series of pioneering works, e.g., digesting moisture as a new hydrogen source for clean energy generation (Zhang et al., 2020a), harvesting moisture-induced electricity energy for self-powered microrobots (Wang et al., 2021), collecting moisture for large-scale urban rooftop farming (Yang et al., 2020). Most interesting are the works revealing that (i) the super-hygroscopic gels capture the moisture thus can block the IR radiation from sun, and (ii) hydrogels can block the mid-IR radiation from buildings to conserve the heat on cold nights (Nandakumar et al., 2018; La et al., 2017). However, besides sweat-triggered electricity harvesting (Zhang et al., 2020b; Mohammadifar et al., 2020), there is still no work that pioneers the utilization of super-hygroscopic gels in capturing face moisture for blocking the self-generated mid-IR radiation for enabling on-faceE to "sustainably" operate at the $T < 0$ °C.

Here, a film enabling On-faceE to work even at −30 °C for 8 h yet without the expense of energy for heating is developed, through pioneering the intelligent conservation and utilization of the waste self-generated heat as a free, sustainable resource. "On-faceE"-oriented fabrication strategies are proposed: (I) one is for making a versatile hydrogel featuring the combined ultra-stretchability, excellent anti-freezing, and adequate breathability simultaneously for preventing heat conduction and part of convection; and (II) another is for enabling the super-hygroscopic gels to capture moisture at the $T < 0$ °C to block mid-IR radiation. The as-fabricated film proves outstanding heat-conserving ability, stability, and sustainability and, importantly, intelligently stops conserving heat as the working $T > 30$ °C, thus solving the two challenges with no expense of energy for heating and positioning it as an energy-saving "smart" T-regulating candidate for conquering low-T limitations for globalizing On-faceE.

2. Results and discussion

2.1. "On-faceE"-oriented fabrication strategy of versatile hydrogel

Ultra-stretchability (>200% Tong et al., 2019b) is essential for sealing On-faceE for conserving heat (the elastic recovery force enables the ultra-stretched film to conform to the complex contour of On-faceE and time-dynamic curvilinear face skin), but super-hygroscopic gels are not stretchable (Nandakumar et al., 2018). To solve this issue, here, the super-hygroscopic gel is coated onto a pre-ultrastretched film followed by releasing ultra-prestrain, generating a waved structure (enduring strain by changing curvature Yang et al., 2019) with stretchability up to the ultra-prestrain level.

Future human-machine interface will base on high-performance alternatives from skin-friendly, renewable, biodegradable bio-sources (Zhou et al., 2019; Yi et al., 2019), so, the stretchability of pure polysaccharide (including cellulose, chitosan, or chitin) hydrogels are summarized (Table S1): (i) among the chemically-crosslinked polysaccharide hydrogels (Zhang et al., 2019; Ye et al., 2019b; Abe and Yano, 2012; Abe et al., 2014; Shi et al., 2014), the free-radical polymerization of the cotton cellulose produced the highest stretchability (129% Abe and Yano, 2012); (ii) among the physically-crosslinked cotton cellulose hydrogels (Zhang et al., 2019; Ye et al., 2019b; Duan et al., 2015; Patchan et al., 2013; Tong et al., 2019a; Liang et al., 2018; Ye et al., 2019a), the metal ion/cellulose coordination led to the highest stretchability (120% Duan et al., 2015); and (iii) so far, the highest stretchability (236% Tong et al., 2019b) has been reached by the double-crosslinks i.e. free-radical polymerization followed by H-bonding. Hence, inspired by the superiority of metal ion/cellulose coordination over H-bonding, there is a reasonable prospect to combine the free-radical polymerization with the metal ion/cellulose coordination to make cellulose hydrogel achieve higher ultra-stretchability.

Here, the "On-faceE"-oriented cellulose hydrogel is made using cotton cellulose dissolved in the $ZnCl_2/CaCl_2$ solution (Fig. 1a), the reasons are as follows: (i) $ZnCl_2$ hydrate exists in the form of ionic liquid $[Zn(OH_2)_6][ZnCl_4]$ with a strong H-bond-donating ability to compete with protons for –OH groups, thus weakening the H-bonding network of cellulose, facilitating Ca^{2+} and water molecules to penetrate cellulose and finally dissolving cellulose (evidenced by the disappearance of X-ray diffraction (XRD) peaks at 14.6°, 16.5°, 34.0° and shift of XRD peak at 22.6° to 20.8°, Fig. 1b) (Duan et al., 2015), and (ii) the –OH groups of dissolved cellulose are then coordinated to Zn^{2+}, Zn-cellulose chains are further locked by Ca^{2+} (see the left dotted box in Fig. 1a), water promotes the coordination equilibrium of Zn^{2+}(the five water molecules filling the 1st hydration shell also attend a 2nd hydration shell) then fill the 2nd hydration shell (Duan et al., 2015). In brief, besides dissolving cellulose, $ZnCl_2$ (freezing point of $ZnCl_2$ aqueous solution can be as low as −73 °C) also attends the physical crosslinks of dissolved cellulose (Zn^{2+}/Ca^{2+}/cellulose coordination) (Duan et al., 2015), endowing the resulting hydrogel with the excellent anti-freezing ability.

Besides, adequate breathability is essential for the use of On-faceE with long-term comfort. The breathability of the cellulose hydrogel rises with the increasing water content (gases diffuse through water Wei et al., 2019). Noteworthily, its stretchability also rises with the increasing water content (water molecules promote the metal ion/cellulose coordination Duan et al., 2015), however, decreases with further increasing the water content (excess water molecules lock the hydrogel network). Hence, adding a suitable amount of water is critical for reaching the highest possible ultra-stretchability under the premise of guaranteeing adequate breathability.

So far, the highest stretchability (236% Tong et al., 2019b) of cellulose hydrogel has been reached by the strategy of firstly chemical crosslinking then physical crosslinking (Table S1) which, however, makes the physical crosslinks occur on the periphery of firstly-formed chemically-crosslinked network (see the upper right dotted box in Fig. 1a), causing inadequate breathability through the main body of hydrogel (gases diffuse through the physically-crosslinked water Wei et al., 2019), so the traditional strategy is not applicable for "On-faceE"-oriented fabrication of versatile hydrogel.

Herein, "On-faceE"-oriented fabrication strategy of versatile hydrogel, i.e., firstly physical crosslinking then chemical crosslinking, is proposed, giving priority to the physical crosslinks to render the adequate and uniformly distributed physically-crosslinked water throughout the hydrogel to guarantee adequate

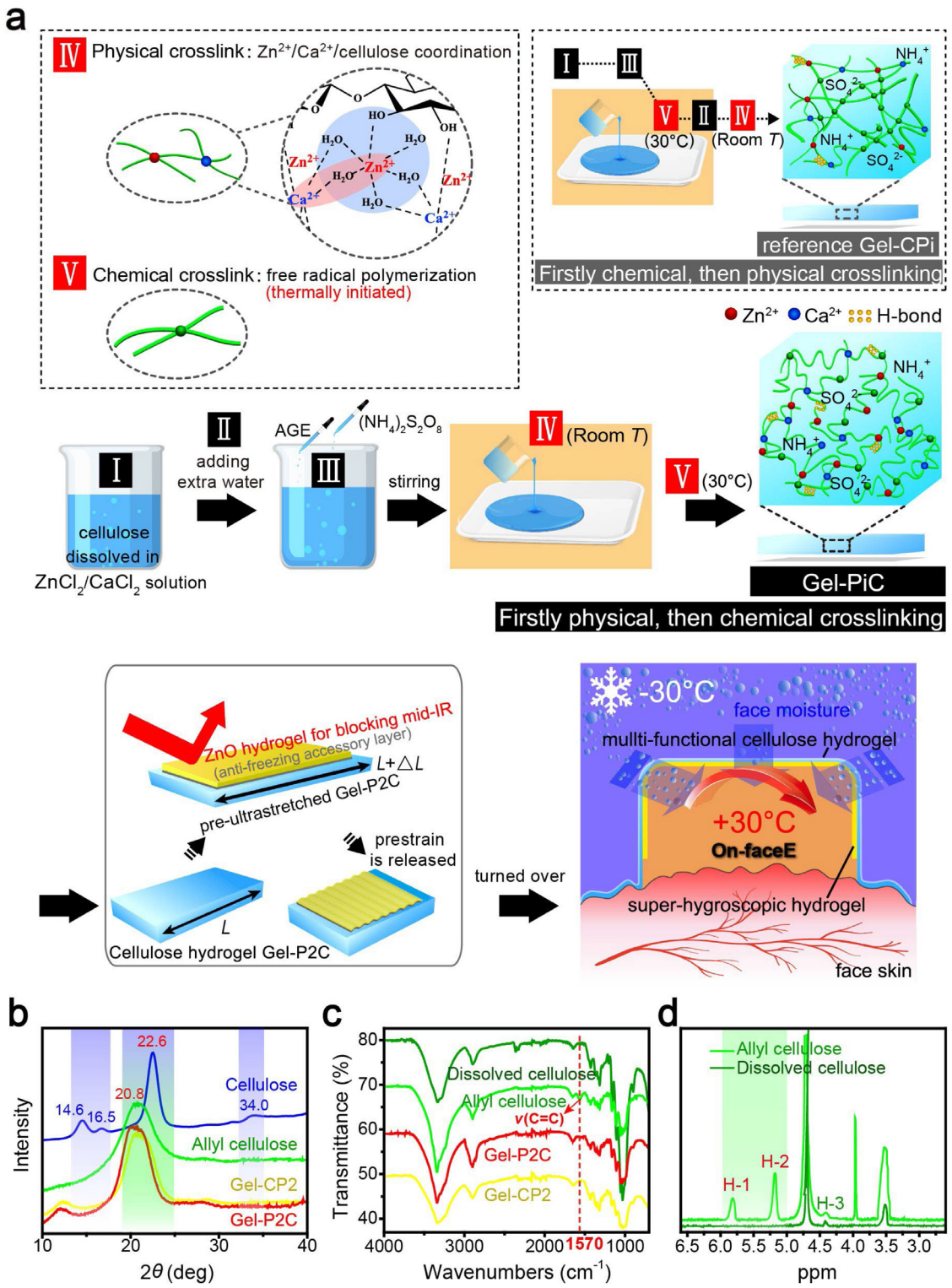

Fig. 1. Film design, working mechanism, and characterization. (a) Schematics of tri-layered film design and the working mechanism enabling On-faceE to sustainably operate at $T < 0$ °C. Spectra of (b) XRD, (c) Fourier transform IR (FTIR), and (d) ^{1}H nuclear magnetic resonance (^{1}H NMR, substitution degree of allyl cellulose is calculated to be 1.73, comparable to reported value Tong et al., 2019b) of cellulose materials.

breathability. Accordingly, "adding a suitable amount of water to induce the Zn^{2+}/Ca^{2+}/cellulose coordination, followed by thermally initiating the free-radical polymerization to achieve the highest possible ultra-stretchability and excellent anti-freezing ability under the premise of guaranteeing adequate breathability" is a feasible "On-faceE"-oriented fabrication mechanism of the versatile cellulose hydrogel.

2.2. The combined ultra-stretchability, excellent anti-freezing, and adequate breathability

Accordingly, the "On-faceE"-oriented fabrication process of versatile cellulose hydrogel is depicted as Step I–V in Fig. 1a: (I) dissolving cellulose in $ZnCl_2/CaCl_2$/water solution, (II) adding different amounts of extra water (physical crosslinker), (III) adding

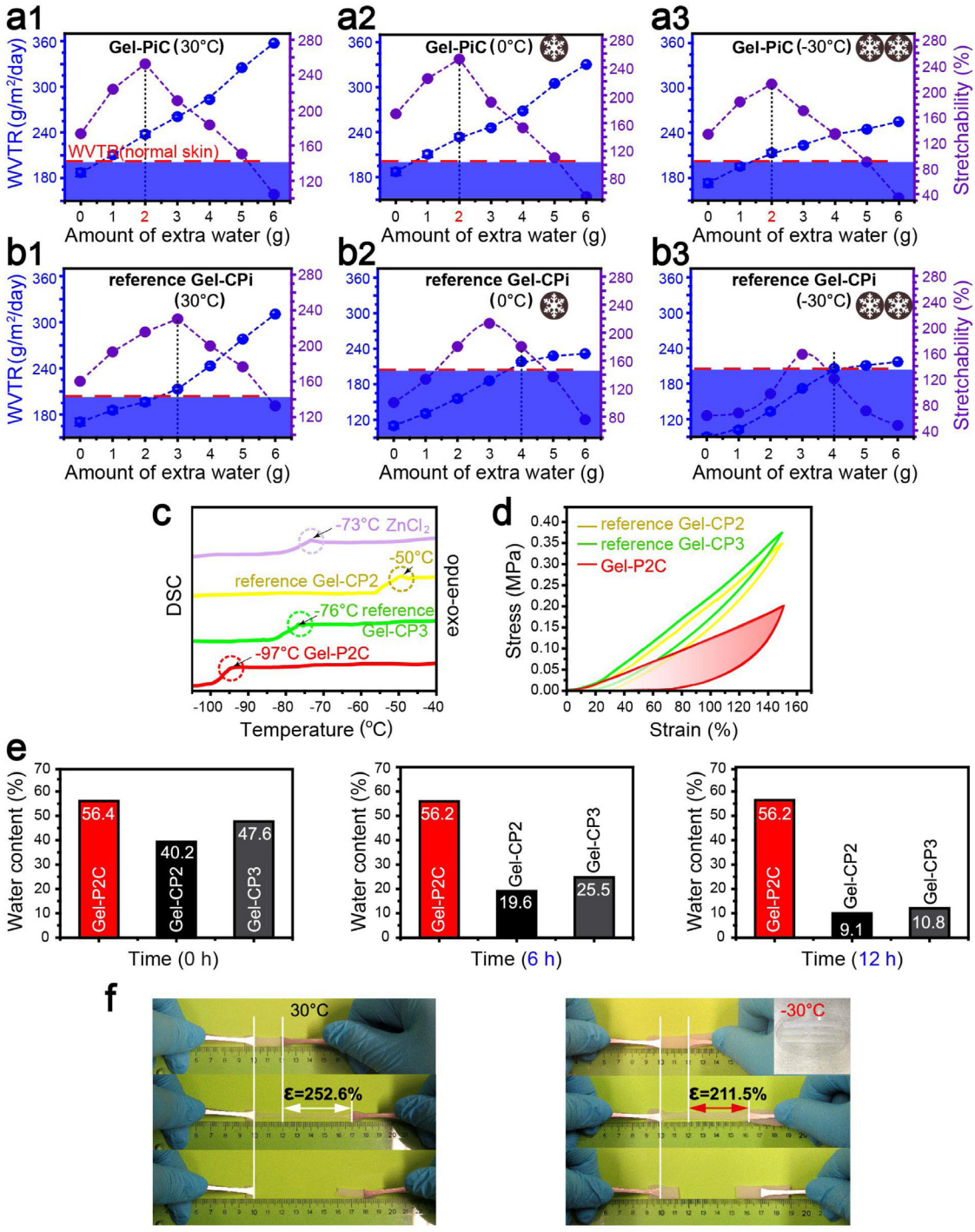

Fig. 2. The combined stretchability, anti-freezing ability, and breathability. Comparison of the stretchability and WVTR between (a) Gel-PiC and (b) reference Gel-CPi (i = 0–6) after exposure to 30, 0, −30 °C for 8 h, the minimum requirement for WVTR is marked by red lines. (c) Dynamic scanning calorimetry (DSC) curves. (d) Tensile stress–strain curves at 150% strain (hydrogel thickness 1 mm, ambient 30 °C). (e) Comparison of water-retaining capacity between Gel-P2C and reference Gel-CPi (i = 2,3) after exposure to 30 °C and 55% relative humidity (RH) for 0, 6, 12 h. (f) A stretched piece of Gel-P2C verifies its excellent anti-freezing ability. . (For interpretation of the references to color in this figure legend, the reader is referred to the web version of this article.)

allyl glycidyl ether (AGE) to modify the dissolved cellulose into allyl cellulose with the C=C bonds (verified by the new peak at 1570 cm^{-1} in FTIR spectrum and new peaks assigned to ethylenic protons H-1 and H-2 in ^{1}H NMR spectra (Ge et al., 2022), Fig. 1c and d), adding $(NH_4)_2S_2O_8$ (chemical crosslinker) and stirring, (IV) keeping the mixture still at 20 °C to let the physical crosslinking proceed, and (V) heating to 30 °C to thermally initiate the chemical crosslinking (confirmed by the disappearance of the peak at 1570 cm^{-1} of C=C bonds, Fig. 1c). The obtained hydrogels are named Gel-PiC (i is the amount of extra water, i = 0–6). Also, the traditional strategy (firstly chemical crosslinking then physical crosslinking) was used to fabricate Gel-CPi (i = 0–6) for reference.

As seen in Fig. 2a1 and Table S1, the Gel-P2C achieves a record-high ultra-stretchability (252.6%) among the pure polysaccharide hydrogels; meanwhile, its breathability, characterized by water vapor transmission rate (WVTR), rises to 235.8 g m^{-2} day^{-1}, surpassing that of normal skin (204 g m^{-2} day^{-1} Zhou et al., 2019). Incorporating more extra water produces Gel-PiC (i >

2) with decreased stretchability (accompanied by markedly increased tensile strength, Fig. S1a1), validating that excess water does lock the network of the hydrogel. Hence, the moderate Zn^{2+}/Ca^{2+}/cellulose coordination induced by the suitable amount of extra water gives rise to the record-high ultra-stretchability and the simultaneously adequate breathability of Gel-P2C.

The anti-freezing ability at an extremely low T of −30 °C is investigated since the average minimum T in January based on NASA's 30-year climatology data collected from typical cities in the northern hemispheres is −25 °C (Wu et al., 2020). As seen in Fig. 2a2 and a3, when T drops to 0 °C, Gel-P2C changes little in the ultra-stretchability and WVTR; when T further drops to −30 °C, Gel-P2C still has ultra-stretchability (>200% Tong et al., 2019b) and adequate WVTR, but Gel-PiC (i > 2) show dramatically decreased stretchability and WVTR. This result verifies that excess water attends Gel-PiC (i > 2) via the H-bonds (with no anti-freezing ability), thus dramatically decreasing the anti-freezing ability; however, the suitable amount of extra water enters Gel-P2C by the Zn^{2+}/ Ca^{2+}/cellulose coordination that imparts the excellent anti-freezing ability to Gel-P2C.

Further DSC studies (Fig. 2c) reveal that Gel-P2C has a freezing point of −97 °C (lower than −3 °C of $ZnCl_2$ aqueous solution owing to $ZnCl_2$/cellulose interaction Duan et al., 2015). Fig. 2f shows that Gel-P2C still has ultra-stretchability even after exposure to −30 °C for 8 h, confirming its excellent anti-freezing ability thus strong application potential for On-faceE.

Our strategy gives priority to the physical crosslinks, verified by larger hysteresis loop of Gel-P2C than those of reference Gel-CP2 and even Gel-CP3 (Fig. 2d, hysteresis loop of tensile loading–unloading curves is due to energy dissipation by de-crosslinking of physical crosslinks Tong et al., 2019b). As the results: (i) "dynamic" dissociation and reassociation of physical crosslinks facilitate the subsequent formation of physical–chemical interpenetrating double-crosslinks, so Gel-P2C has higher stretchability (Fig. 2a and b) than reference Gel-CP2 and even Gel-CP3 where "fixed" chemically-crosslinked network hinders the subsequent formation of chemical–physical interpenetrating double-crosslinks; (ii) the higher dispersity of Zn^{2+} and more sufficient Zn^{2+}/ Ca^{2+}/cellulose coordination lead to the lower freezing point thus higher anti-freezing ability of Gel-P2C than those of reference Gel-CP2 and even Gel-CP3 (Fig. 2c); and (iii) more adequate, uniformly distributed physical-crosslinks lock in more water and prevent the volatilization loss of water (Duan et al., 2015), rendering higher water-retaining capacity (Fig. 2e) thus higher WVTR of Gel-P2C than those of reference Gel-CP2 and even Gel-CP3 (Fig. 2a and b). All in all, the superiority of our strategy over traditional strategy endows Gel-P2C with the combined ultra-stretchability, excellent anti-freezing, and adequate breathability simultaneously.

2.3. "On-faceE"-oriented fabrication mechanism of tri-layered film For heat conservation

The emerging hygroscopic gels are propelling a series of pioneering works (Zhang et al., 2020a; Wang et al., 2021; Yang et al., 2020), yet are prone to freeze. The lack of anti-freezing ability hinders their widespread applications and thus is a weakness that must urgently be improved. Recently, ZnO gel with atom ratio Zn/O = 1/1.1 was proved to strongly capture moisture (as high as 420% of its weight after exposure to 90% RH for 24 h) (Nandakumar et al., 2019). Density Function Theory calculation showed that when the number of water molecules adhered to ZnO gel rises beyond 120, the binding energy of water molecules with ZnO gel becomes zero, indicating that most absorbed water molecules are "physically adsorbed" and not chemically bound to ZnO gel (Nandakumar et al., 2018). This result urges us to use an anti-freezing agent to form H-bonds with the physically-adsorbed water molecules to disrupt ice crystal formation (Duan et al., 2015; Liao et al., 2019). We selected glycerol, a nontoxic, anti-freezing, hygroscopic agent, to lower the freezing point as well as increase the hygroscopicity. However, even if mixing 66.7 wt% glycerol–water agent, whose freezing point is as low as −46.5 °C, into ZnO gel, the overall freezing point would still rise to surpass the ambient T (e.g., −30 °C, Table S2) after ZnO gel captures moisture. And more importantly, anti-freezing agents (including glycerol) have far lower hygroscopicity than super-hygroscopic ZnO gel, so mixing an anti-freezing agent into ZnO gel would separate ZnO gel into isolated domains (small water-rich domains "transmit" mid-IR radiation La et al., 2017), destroying the mid-IR-blocking ability of ZnO hydrogel.

Considering that (i) the conserved "steady stream" of self-generated heat would keep the hygroscopic hydrogel from freezing as long as preventing hygroscopic gel (in the dehydrated state) from freezing at the very beginning, and (ii) super-hygroscopic gel can super-fast capture moisture for heat conservation at the very beginning (Fig. 3a and b, ZnO gel captures moisture far faster than the commercial desiccant calcium chloride or silica gel), we propose that "coating (instead of mixing) an anti-freezing accessory layer" is a feasible "On-faceE"-oriented strategy enabling the super-hygroscopic gels to capture moisture at the T < 0 °C.

As seen in Fig. 3c, the as-prepared (66.7 wt% glycerol–water film/ZnO gel) bilayered film has a freezing point of −46.5 °C @ t = 0 min, confirming that the 66.7 wt% glycerol–water film layer (freezing point: −46.5 °C) dominates the overall freezing point @ t = 0 min. Of note, the depressing effect on the ice formation works at the interface of the bilayered film thus would gradually go out of action due to the increasing ZnO hydrogel thickness after capturing moisture. Hence, "coating 66.7 wt% glycerol–water film and a 'suitable thickness' of ZnO gel in sequence onto 252.6% pre-ultrastretched Gel-P2C then releasing prestrain to get a tri-layered film, which can super-fast capture moisture for heat conservation at the very beginning before the freezing point of (ZnO gel/66.7 wt% glycerol–water film) bilayers surpassing the ambient T" is a feasible "On-faceE"-oriented fabrication mechanism of the film for heat conservation.

The effect of ZnO gel thickness on the moisture capture rate at the beginning was studied since "thin" hygroscopic gel captures moisture faster while "thick" hygroscopic gel captures more moisture (Nandakumar et al., 2020). As seen in Fig. 3d, the thinnest ZnO gel (370 cm^2 g^{-1}) captures moisture fast, but the resultant ZnO hydrogel would have not enough mid-IR-blocking ability (Fig. S2); while thick ZnO gel (170 or 80 cm^2 g^{-1}) captures moisture slowly (diffusion of water molecules from surface to bottom is slower than moisture capture Nandakumar et al., 2020). As far as the ZnO gel (350 cm^2 g^{-1}) is concerned, the resulting (66.7 wt% glycerol–water film/ZnO gel) bilayered film captured moisture as high as 87% of its weight in the beginning 3 min (Fig. 3b) before the whole freezing point of bilayered film surpassing the ambient T of −30 °C (see the black dotted line in Fig. 3c) and would have high mid-IR-blocking ability (Fig. S2) for conserving heat (discussed later). Hence, in this work, the (surface area/weight) ratio of ZnO gel is set to be 350 cm^2 g^{-1}.

2.4. Intelligent heat conservation and waste heat utilization

The hygroscopicity under different (RH, T) of as-fabricated (ZnO gel/66.7 wt% glycerol–water film/Gel-P2C) tri-layered film was studied. As seen in Fig. 3f, hygroscopicity is sensitive to RH: a linear stage (RH < 40%), a nonlinear stage (40% < RH < 60%), and a nonlinear stage with a sharply increased capture amount (RH > 60%). After exposure to 90% RH for 3 min, the

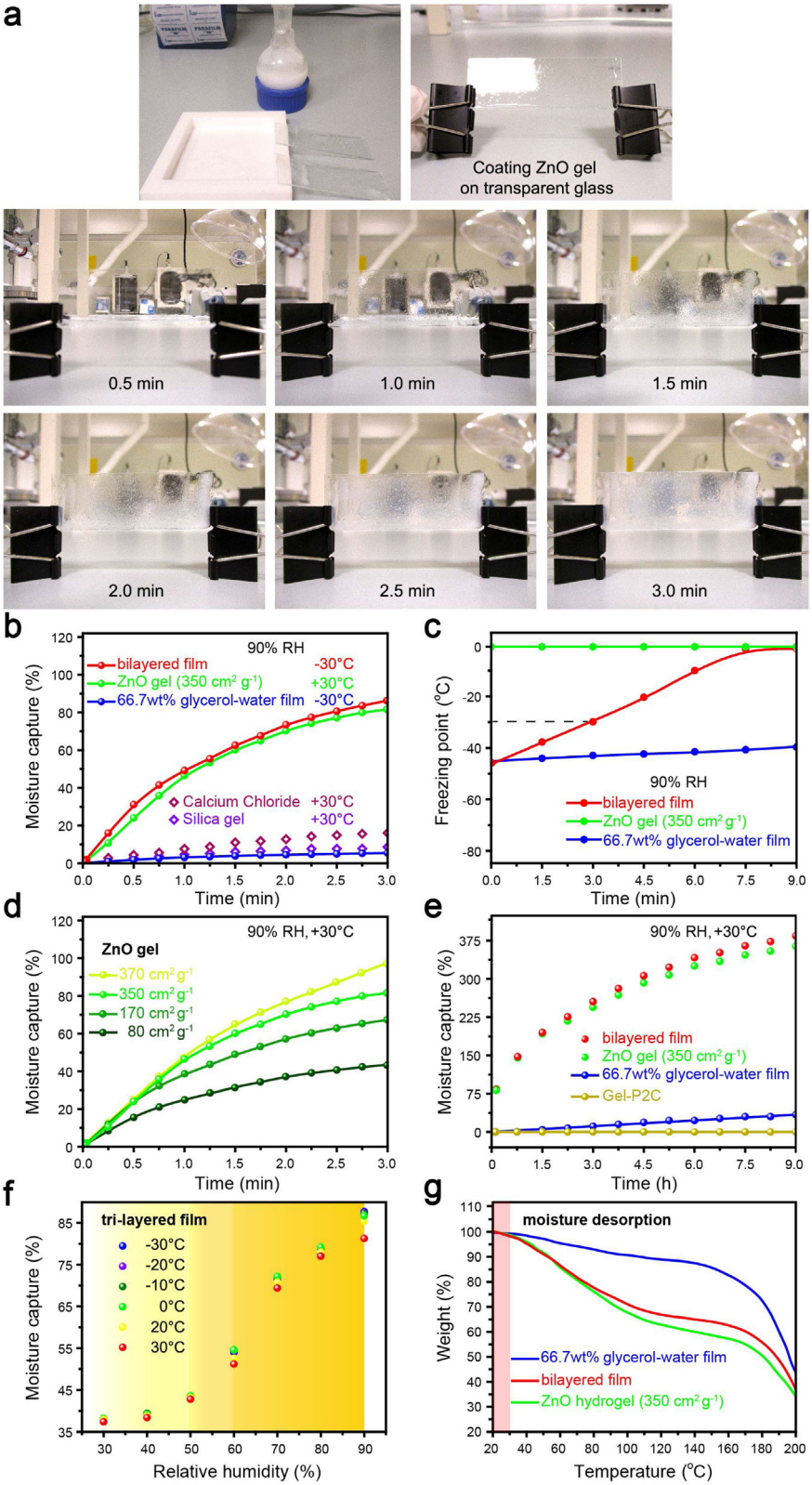

Fig. 3. Moisture capture/desorption and freezing point. (a) Super-fast speed of ZnO gel in capturing moisture (ambient 90% RH, 25 °C). In the beginning 3 min, (66.7 wt% glycerol–water film/ZnO gel) bilayered film (b) captured moisture as high as 87% of its weight (ambient 90% RH, −30 °C) and as a result, (c) its freezing point rose to approach ambient T (−30 °C). (d) Effect of ZnO gel thickness on the moisture capture rate at the beginning. Hygroscopicity of (e) each layer and (66.7 wt% glycerol–water film/ZnO gel) bilayered film in 9 h, and (f) tri-layered film under different (RH, T) for 3 min. (g) Thermogravimetric analyzer (TGA) curves.

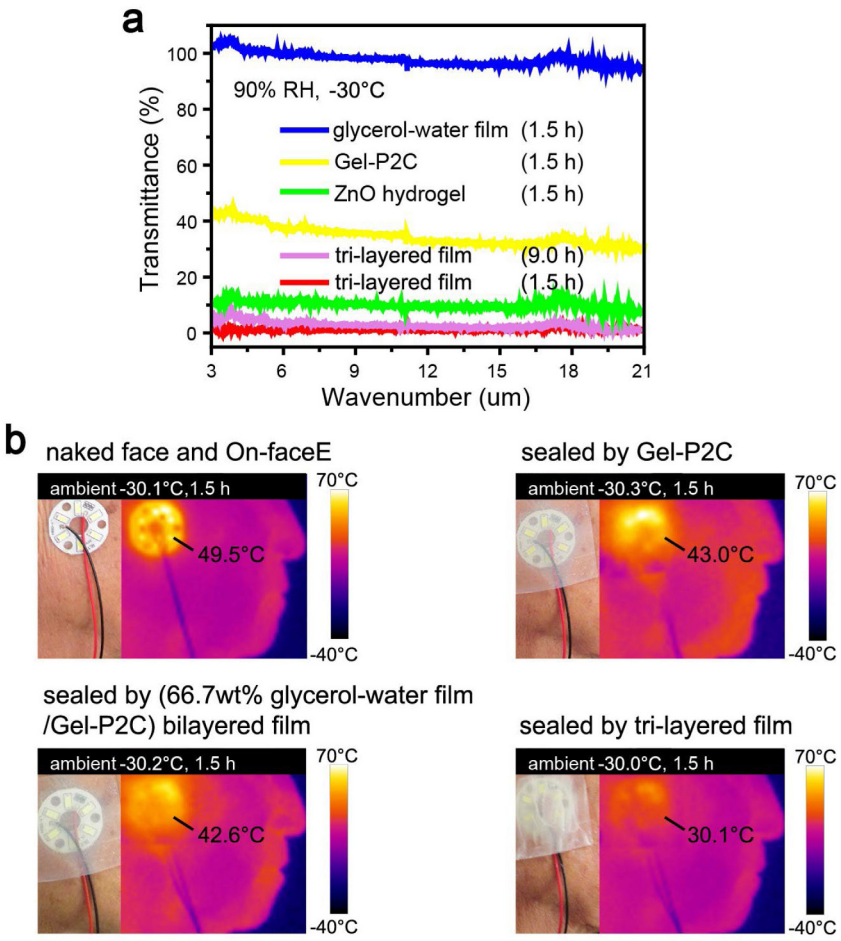

Fig. 4. Mid-IR radiation transmittance and heat-conserving ability. (a) Mid-IR radiation transmittance through each layer (1 mm thick) or tri-layered film (3 mm thick) after sealing On-faceE for 1.5 h or 9 h (exposure to 90% RH within face mask, ambient (−30 °C, 50% RH)). (b) Optical and mid-IR images of On-faceE before and after being sealed for 1.5 h by Gel-P2C, (66.7 wt% glycerol–water film/Gel-P2C) bilayered film, or tri-layered film, ambient (−30 °C, 50% RH).

hygroscopicity had risen to 87% of its weight, equal to that of (ZnO gel/66.7 wt% glycerol–water film) bilayered film (Fig. 3b), confirming that physical crosslinks with water molecules had completed during the fabrication of Gel-P2C by using our strategy. More importantly, the hygroscopicity is insensitive to T yet except the declines at 30 °C (due to heat-driven moisture desorption (Zhang et al., 2020b), see TGA curves in Fig. 3g), this not only evidences the wide T applicability of our tri-layered film (−30 °C to 30 °C) but highlights its "intelligent" heat conservation ability as it stops conserving heat when the working $T > 30$ °C.

Absorbing or reflecting mid-IR radiation conserves self-generated heat for On-faceE, yet transmitting mid-IR radiation (can be tested by FTIR) loses heat. Fig. 4a reveals that the average transmittance of mid-IR radiation through each layer follows a sequence: ZnO hydrogel (9.7%) < Gel-P2C (36.2%) < 66.7 wt% glycerol–water film (97.1%). According to water-triggered IR blocking mechanisms: (I) water "absorbs" mid-IR radiation, and (II) large macroscopic water-rich domains "backscatter" electromagnetic light, but small water-rich domains "transmit" light (La et al., 2017), it can be concluded that: (i) 66.7 wt% glycerol–water film has the least water thus the lowest mid-IR-blocking ability; (ii) Gel-P2C has slightly less water yet blocks far less mid-IR radiation (56 wt% water, 36.2% transmittance) than ZnO hydrogel (65.2 wt% water, 9.7% transmittance), verifying that our strategy makes physical crosslinks uniformly distribute in Gel-P2C (isolating small water-rich domains which transmit light); and (iii) owing to the highest water content (65.2 wt%, comparable to the reported value Nandakumar et al., 2019) and the large macroscopic water-rich domains after capturing moisture (187.2% of its weight, Fig. 3(e)), ZnO hydrogel layer has the highest mid-IR-blocking ability.

Profited from the synergistic effect of three layers, our tri-layered film blocks 99.3% mid-IR radiation after on-face exposure to 90% RH for 1.5 h and still blocks 99% mid-IR radiation even after 9 h (ambient −30 °C, Fig. 4a), giving strong evidence to support our hypothesis that as long as preventing ZnO gel layer from freezing at the very beginning, the conserved "steady stream" of self-generated heat would keep our tri-layered film from freezing afterward.

The heat-conserving ability is further evaluated using a heat-sensing mid-IR radiometer camera. As seen in Fig. 4b, On-faceE can be imaged by the camera after being sealed by Gel-P2C or (66.7 wt% glycerol–water film/Gel-P2C) bilayered film, yet is ∼50% invisible to the camera after being sealed by (ZnO hydrogel/66.7 wt% glycerol–water film/Gel-P2C) tri-layered film, verifying that the ZnO hydrogel layer dominates the heat-conserving ability. Noteworthily, On-faceE is only ∼10% invisible to the camera after being sealed by a commercial cotton face mask with the same thickness (see Fig. 5a), evidencing that our tri-layered film dramatically outperforms the commercial cotton face mask in conserving the self-generated heat.

Wearing one 3 mm-thick commercial cotton face mask gathers the respiration moisture, easily increasing the humidity within the mask to 90% RH regardless of the subject's gender, age, and metabolic status (there is no need to use multiple masks). After being sealed by our tri-layered film + face mask, not only the

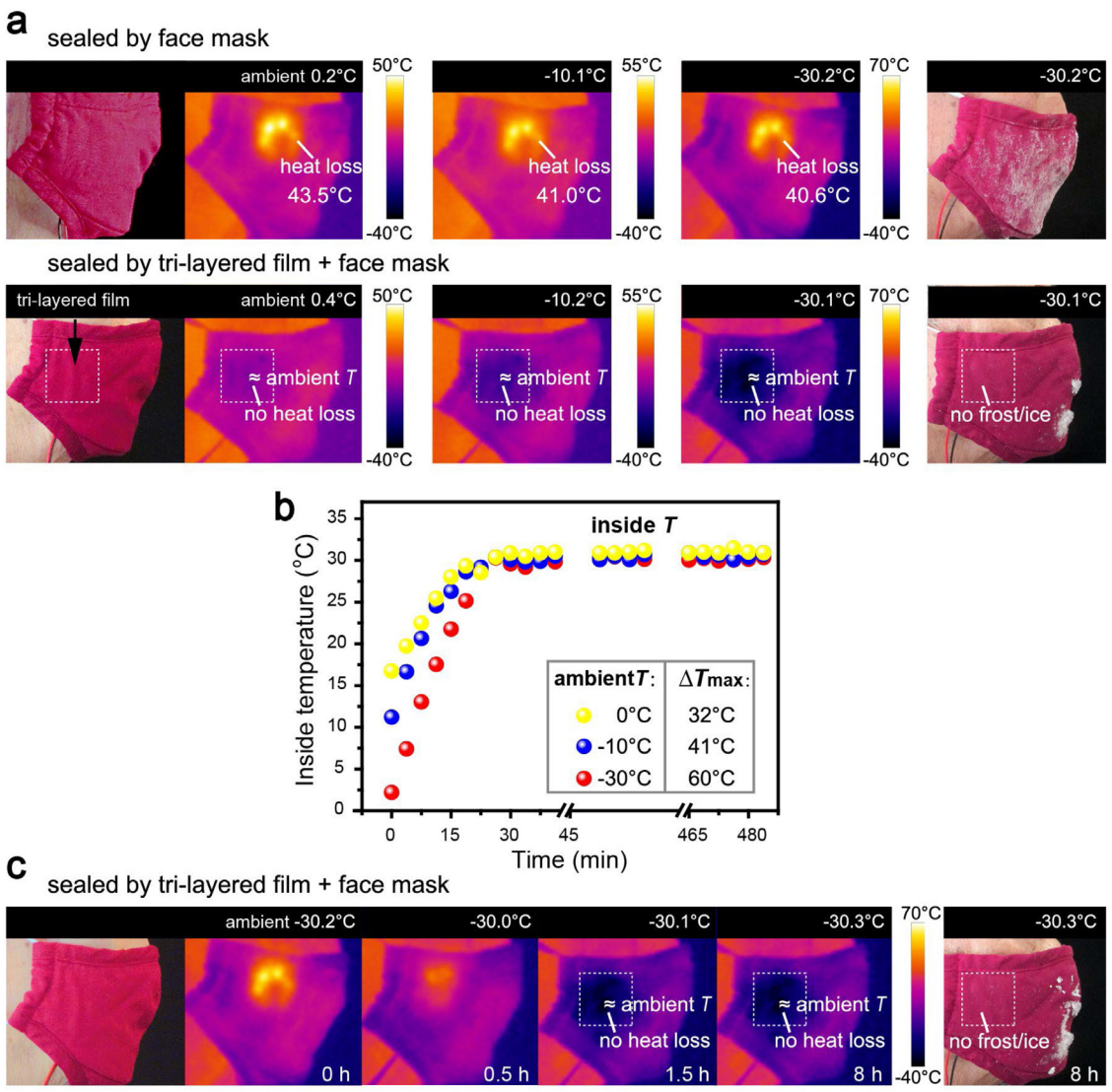

Fig. 5. Heat conservation and utilization. (a) Optical and mid-IR images of On-faceE after being sealed by a commercial cotton face mask (3 mm thick) or tri-layered film + face mask for 1.5 h when ambient $T \approx 0$, -10, -30 °C; (b) Time dependence of the T inside the space enclosed by face skin (25 cm^2) and tri-layered film + face mask, and the maximum ΔT (ΔT_{max}) between inside T and ambient T (≈ 0, -10, -30 °C); (c) Optical and mid-IR images of On-faceE after being sealed by tri-layered film + face mask for 0, 0.5, 1.5, 8 h (ambient -30 °C). The ambient humidity is ~50% RH, and the humidity within face mask is ~90% RH.

On-faceE but the skin underneath is 99% invisible to the mid-IR radiometer camera (Fig. 5a, ambient $T \approx 0$, -10, -30 °C), yet meanwhile, the T (tested by electronic thermometer) inside the space enclosed by face and tri-layered film + face mask is about 30 °C (Fig. 5b), confirming that the face moisture (gathered by mask then captured by super-hygroscopic ZnO gel layer) plays an important role in the waste heat utilization.

When extending the working time to 8 h to fit the world's universal 8-h working system (ambient -30 °C), On-faceE became invisible to the mid-IR radiometer camera and no frost/ice accretion appeared around the tri-layered film (see the dashed box on the face mask, Fig. 5c); meanwhile, the T inside the space enclosed by face and tri-layered film + face mask rose to and kept at 30 °C (Fig. 5b). This reconfirms that our tri-layered film captured face moisture (helps prevent the frost/ice accretion) and harnessed the "steady stream" self-generated face moisture in conserving the "steady stream" self-generated heat, successfully solving the two challenges: sustainable operation at the $T < 0$ °C and frost/ice accretion security hazard.

Though ZnO gel needs more than 9 h to saturate with moisture under 90% RH (Fig. 3e) (Nandakumar et al., 2019), the unsaturated ZnO hydrogel layer after capturing 30 min moisture has already enabled our tri-layered film to utilize the conserved heat to enhance the inside T to 30 °C after sealing On-faceE (Fig. 5b, this T rise process can be accelerated if people speaks or exhales using the mouth as the humidity within mask would rise to 100% RH) and, importantly, intelligently stops conserving heat (switching from moisture capture to desorption, Fig. 3g) when the working $T > 30$ °C. As a result, a ΔT of 60 °C between inside T and ambient T (-30 °C) can sustain >8 h (Figs. 4a and 5b), meeting the world's universal 8-h working system. Altogether, such intelligent heat conservation and waste heat utilization position our tri-layered film as an energy-saving "smart" T-regulating candidate for On-faceE.

2.5. Self-healing promoted by conserved heat; heat-conserving stability and sustainability

Under tension, dissociation of the physical crosslinks and deformation of the chemically-crosslinked networks of Gel-P2C layer dissipate energy. As unloading, permanent deformation occurs in the chemically-crosslinked networks. The self-healing

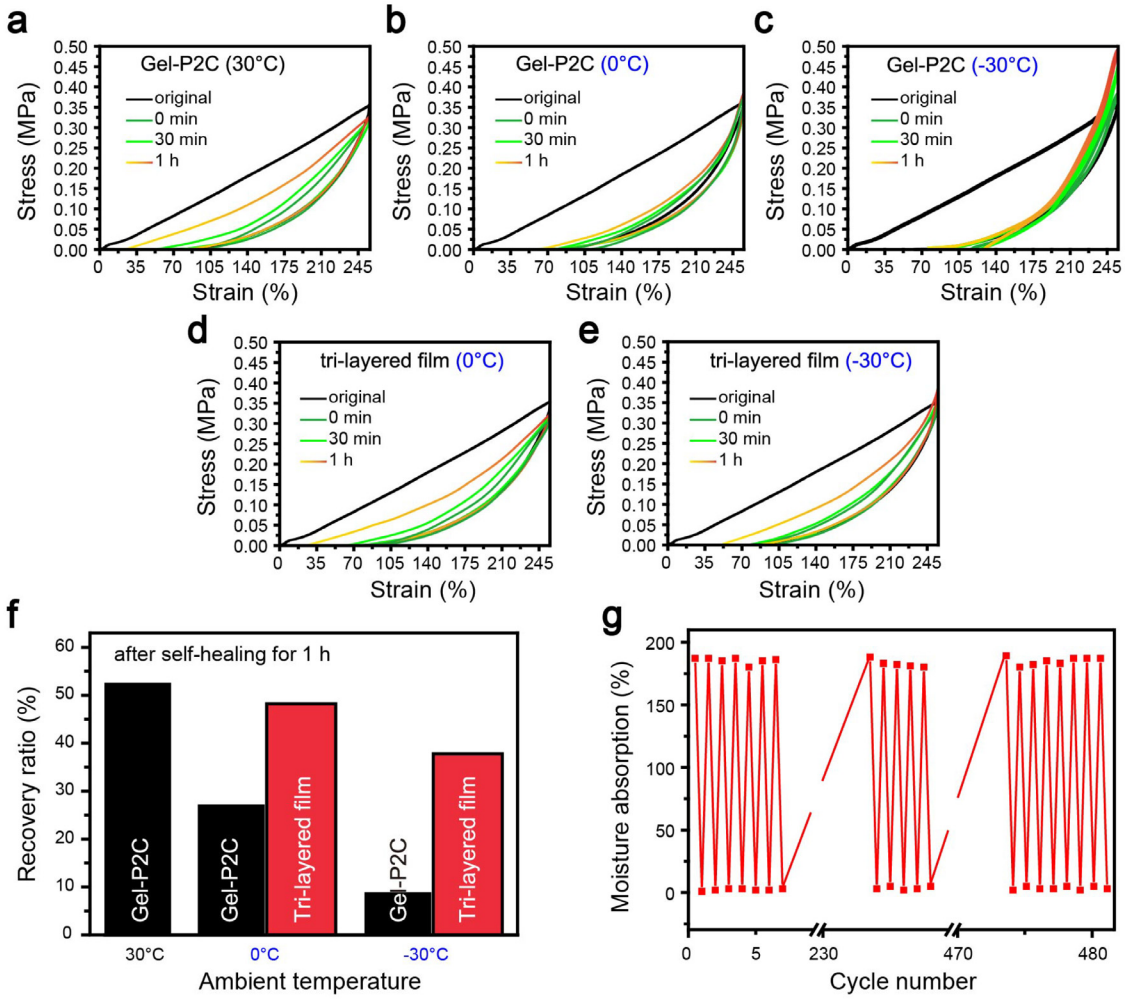

Fig. 6. Self-healing ability, heat-conserving stability and durability. Cyclic tensile loading–unloading curves at 252.6% strain after different self-healing times (under 90% RH within face mask) of Gel-P2C layer when ambient T is (a) 30 °C, (b) 0 °C, (c) −30 °C and of tri-layered film when ambient T is (d) 0 °C, (e) −30 °C. (f) Comparison of self-healing recovery ratio between Gel-P2C layer and tri-layered film. (g) Capturing-desorbing moisture cyclic performance of tri-layered film (exposure to 90% RH within face mask for 1.5 h when ambient $T \approx -30$ °C, then exposure to 110 °C for 2 h for desorbing moisture; repeating this cycle >480 times).

by reassociation of the physical crosslinks endows Gel-P2C layer with the reversible stretchability (Tong et al., 2019b), making our tri-layered film competent in subjecting to repeated tension-unloading cycles exerted by time-dynamic face skin. Notably, internal damage could not self-heal immediately after releasing prestrain, so we compared the self-healing ability between the Gel-P2C layer and tri-layered film by testing cyclic tensile loading–unloading curves after different self-healing times. The recovery ratio was defined as the ratio of energy dissipation ($R_{ed} = \int_{\text{loading}} \sigma \mathrm{d}\varepsilon - \int_{\text{unloading}} \sigma \mathrm{d}\varepsilon$, where σ is the tensile stress and ε is the tensile strain during the cycle) to the original curve (Tong et al., 2019b). As seen in Fig. 6a–c,f and Fig. S3, the stress–strain curves of Gel-P2C layer gradually recovered with increasing self-healing time, after self-healing for 1 h, the recovery ratio climbed to 52.3% when ambient $T \approx 30$ °C, yet only rose to 26.9% when the ambient $T \approx 0$ °C and 8.6% when the ambient $T \approx -30$ °C. By contrast, the recovery ratio of the tri-layered film rose to 48.2% when the ambient $T \approx 0$ °C and 37.8% when the ambient $T \approx -30$ °C (Fig. S3). Our tri-layered film exhibits higher self-healing ability than its Gel-P2C layer when the ambient $T <$ 0 °C (Fig. 6d–f), indicating that the self-generated heat conserved by our tri-layered film, in turn, promotes the self-healing of its Gel-P2C layer when the ambient $T < 0$ °C.

Our film has a stable and sustainable hygroscopicity with negligible hygroscopicity loss even after undergoing 480 capturing-desorbing moisture cycles when the ambient T is as low as −30 °C (Fig. 6g). This result indicates that the conserved "steady stream" of self-generated heat not only keeps the ZnO hydrogel layer from freezing but also guarantees its high cyclic performance in capturing-desorbing moisture at the $T < 0$ °C. Besides, as estimated in Table S3, producing our tri-layered film costs less than 0.65 $ per 25 cm^2. To sum up, our tri-layered film with low cost also demonstrates outstanding heat-conserving stability and sustainability.

3. Conclusion

In summary, through pioneering the intelligent conservation and utilization of waste self-generated heat, a film enabling On-faceE to work even at −30 °C for 8 h yet without the expense of energy for heating is demonstrated. This work has three innovative aspects: (1) this is the first attempt at utilizing the waste self-generated heat and face moisture as free, sustainable resources for On-faceE to sustainably operate at the $T < 0$ °C; (2) "On-faceE"-oriented general fabrication strategies are developed, instructive for controlling film properties; (3) the film creates a ΔT up to 60 °C between inside T and ambient T (−30 °C)

after sealing On-faceE and intelligently stops conserving heat when the working $T > 30$ °C and also demonstrates outstanding heat-conserving stability and durability, thus positioning it as an energy-saving "smart" T-regulating candidate. Altogether, successfully solving the two challenges (sustainable operation at the $T < 0$ °C and frost/ice accretion security hazard) without the expense of energy for heating, this film with low cost could address the energy shortage and heating costs for breaking through various low-T limitations (winter, cold nights, and low-T regions e.g., high altitude, deep-sea) for globalizing On-faceE and opens up a new route to develop "zero-energy" On-faceE.

4. Experimental section

4.1. Fabrication of versatile cellulose hydrogel layer

(i) $ZnCl_2$ (19.7 g, 99.0%) and $CaCl_2$ (0.4 g, 99.0%) were dissolved in deionized (DI) water (7.3 g) at 75 °C, then cotton linter pulp (0.4 g, 1.2 wt%, α-cellulose content >96%) was added and dissolved after vigorously stirring for 30 min (Duan et al., 2015); (ii) a desired dosage (based on the weight of DI water) of NaOH (7 wt% (Ge et al., 2022), acting as reaction medium) was added for the etherification of dissolved cellulose, then AGE (99%) was added into the stirred solution (30 °C for 24 h Ge et al., 2022) until a desired molar ratio (8.0 Tong et al., 2019b) of AGE to the anhydroglucose unit of cellulose was reached, the mixture was washed thrice using anhydrous ether (30 mL anhydrous ether per 10 g of mixture solution) to remove residual AGE and rotarily evaporated at 30 °C for 1 h to remove residual ether; (iii) $(NH_4)_2S_2O_8$ (99.9%, 1.0 wt% based on the weight of cellulose solution Tong et al., 2019b) and different amounts (i = 0, 1, 2, 3, 4, 5, 6 g) of extra DI water were added and stirred followed by centrifugation (8000 rpm, 1 min) to remove air bubbles; (iv) the mixture was poured into molds, maintained at 20 °C for 24 h for the physical crosslinking, then kept at 30 °C for 24 h to thermally initiate the chemical crosslinking. The as-fabricated hydrogel was denoted as Gel-PiC (i = 0–6, i is the extra water amount). In addition, reference Gel-CPi (i = 0–6) were fabricated by keeping the mixture at 30 °C for 24 h to thermally initiate the chemical crosslinking then maintaining it at 20 °C for 24 h to let the physical crosslinking proceed.

4.2. Fabrication of tri-layered film

Zinc acetate dehydrate (0.7 M) and ethanolamine (84 μL) were added in 2-methoxyethanol (2 mL), the solution was sonicated for 20 min until Zinc acetate dehydrate was dissolved and a clear transparent ZnO gel (dehydrated state) was obtained. 66.7 wt% glycerol–water film and ZnO gel were coated in sequence onto pre-ultrastretched cellulose hydrogel. After releasing prestrain, the obtained (ZnO gel/66.7 wt% glycerol–water film/Gel-P2C) tri-layered film was turned over to seal On-faceE.

It is worth noting that (i) high concentrations of glycerol can clog the pores of the skin and dehydrate the skin, and (ii) Zinc oxide is used to make ointments for clinical treatment of skin damage; it can help relieve itching and promote blood circulation, but people with allergic constitution cannot use zinc oxide ointment, and what is more, ZnO gel (dehydrated state) can dehydrate the skin. Hence, the 66.7 wt% glycerol–water film layer and the ZnO gel layer of tri-layered film can only touch On-faceE, not the skin. Besides, the health hazards of zinc ions are inhalation of zinc mist or ingestion of excessive zinc. In this work, Gel-P2C is prepared at 30 °C for 24 h and our tri-layered film intelligently stops conserving heat when the working $T > 30$ °C as aforementioned, so Zn^{2+} exist stably in the Gel-P2C layer in the form of Zn^{2+}/Ca^{2+}/cellulose coordination thus do not cause irritation to the skin or health hazards. To sum up, our tri-layered film should seal On-faceE by clinging to skin with its Gel-P2C layer.

4.3. Characterizations

The dissolution of cellulose was testified by XRD (D8 Davinci, Bruker). The modification of dissolved cellulose into allyl cellulose with C=C double bonds was verified by FTIR (Perkin-Elmer Frontier) and ^{1}H NMR (recorded in D_2O on 400 MHz Ultrashielded Bruker Avance III NMR spectrometer), the substitution degree was estimated by $(S_{H\text{-}1} + S_{H\text{-}2})/3/S_{H\text{-}3}$, where $S_{H\text{-}3}$ is digital integral of ^{1}H NMR signals arising from the alpha anomeric proton of glucose residues, as well as $S_{H\text{-}1}$ and $S_{H\text{-}2}$ of ethylenic protons (Ge et al., 2022). Before structural characteristics of allyl cellulose, the mixture was precipitated and washed thrice with acetone (30 mL of acetone per 10 g of mixture solution), purified allyl cellulose was got after being dialyzed in DI water and freeze-dried. Cellulose hydrogels for XRD and FTIR characterization were freeze-dried after being thoroughly washed by DI water to remove impurities. Tensile tests were done on samples (8×60 mm^2 $\times$ 2 mm thickness) by Instron 5549 system (500 N load cell, 10 mm min^{-1} tension rate), fixtures and samples were taken out from the freezer and tested immediately. Each test was repeated six times. Freezing points were tested using DSC (214 Netzsch tester), samples were cooled at a rate of 10 °C min^{-1} to −150 °C, kept for 15 min, then heated to 30 °C at a rate of 10 °C min^{-1}. WVTR was measured using the method described in Ref. Zhou et al. (2019) based on standard ASTM E96-05. Moisture absorption tests were done on an AquaLab Vapor Sorption Analyzer. After samples had been exposed to 90% RH for 1 h, TGA tests were conducted using a thermal analyzer (Perkin-Elmer) with a ramping rate (2 °C min^{-1}) under N_2 flow. As the maximum mid-IR radiation of black body with −73 °C, 27 °C, 87 °C occurs at 8, 10, and 15 μm, respectively (Moghimi et al., 2018), mid-IR transmittance spectra covering a wider range (3–21 μm) were investigated using FTIR spectrophotometer (Nicolet 8700, Thermo), samples (1 mm thick) were stabilized at the desired T in the freezer for 1 h before measurement. A mid-IR camera (FLIR T620, the T range of the tested object −40 °C∼650 °C) was used to detect and image the heat radiation.

CRediT authorship contribution statement

Tianle Zhou: Conceptualization, Experiment, Data analysis, Writing – review & editing. **Zheng-Dong Chen:** Experiment Assistant. **Shuang-Qin Chen:** Experiment, Data analysis. **Feng Wang:** Background, Experiment, Data analysis. **Yizhi Zhuo:** Experiment, Data analysis. **Zhiliang Zhang:** Conceptualization, Experiment, Project administration. **Jianying He:** Conceptualization, Experiment. **Huaping Tan:** Experiment, Data analysis. **Xiaoheng Liu:** Conceptualization, Experiment. **Xin Wang:** Conceptualization.

Declaration of competing interest

The authors declare that they have no known competing financial interests or personal relationships that could have appeared to influence the work reported in this paper.

Acknowledgments

The Research Council of Norway is acknowledged for the support to the Norwegian Micro- and Nano-Fabrication Facility, NorFab, project number 245963/F50. This work was also supported by China Scholarship Council (CSC) for Visiting Scholar Overseas Research Program, Priority Academic Program Development of Jiangsu Higher Education Institutions (PAPD) of China, and Natural Science Foundation of Jiangsu Province of China (Grant No. BK20190480).

Appendix A. Supplementary data

Supplementary material related to this article can be found online at https://doi.org/10.1016/j.egyr.2022.05.024.

References

Abe, K., Ifuku, S., Kawata, M., Yano, H., 2014. Preparation of tough hydrogels based on β-chitin nanofibers via NaOH treatment. Cellulose 21, 535–540. http://dx.doi.org/10.1007/s10570-013-0095-0.

Abe, K., Yano, H., 2012. Cellulose nanofiber-based hydrogels with high mechanical strength. Cellulose 19, 1907–1912. http://dx.doi.org/10.1007/s10570-012-9784-3.

Duan, J., Liang, X., Cao, Y., Wang, S., Zhang, L., 2015. High strength chitosan hydrogels with biocompatibility via new avenue based on constructing nanofibrous architecture. Macromolecules 48, 2706–2714. http://dx.doi.org/10.1021/acs.macromol.5b00117.

Ge, W., Shuai, J., Wang. Y. Zhou, Y., Wang, X., 2022. Progress on chemical modification of cellulose in green solvents. Polym. Chem. 13, 359–372. http://dx.doi.org/10.1039/D1PY00879J.

Kim, JJ., Wang, Y., Wang, H., Lee, S., Yokota, T., Someya, T., 2021. Skin electronics: next-generation device platform for virtual and augmented reality. Adv. Funct. Mater. 31, 2009602. http://dx.doi.org/10.1002/adfm.202009602.

La, T., Li, X., Kumar, A., Fu, Y., Yang, S., Chung, H., 2017. Highly flexible, multipixelated thermosensitive smart windows made of tough hydrogels. ACS Appl. Mater. Interfaces 9, 33100–33106. http://dx.doi.org/10.1021/acsami.7b08907.

Liang, X., Wang, X., Xu, Q., Lu, Y., Zhang, Y., Xia, H., Lu, A., Zhang, L., 2018. Rubbery chitosan/carrageenan hydrogels constructed through an electroneutrality system and their potential application as cartilage scaffolds. Biomacromolecules 19, 340–352. http://dx.doi.org/10.1021/acs.biomac.7b01456.

Liao, H., Guo, X., Wan, P., Yu, G., 2019. Conductive mxene nanocomposite organohydrogel for flexible, healable, low-temperature tolerant strain sensors. Adv. Funct. Mater. 29, 1904507. http://dx.doi.org/10.1002/adfm.201904507.

Lim, H., Kim, HS., Qazi, R., Kwon, Y., Jeong, J., Yeo, W., 2020. Advanced soft materials, sensor integrations, and applications of wearable flexible hybrid electronics in healthcare, energy, and environment. Adv. Mater. 32, 1901924. http://dx.doi.org/10.1002/adma.201901924.

Liu, Y., Zhang, S., Zhou, Y., Buckingham, MA., Aldous, L., Sherrell, PC., Wallace, GG., Ryder, G., Faisal, S., Officer, DL., Beirne, S., Chen, J., 2020. Advanced wearable thermocells for body heat harvesting. Adv. Energy Mater. 10, 2002539. http://dx.doi.org/10.1002/aenm.202002539.

Moghimi, MJ., Lin, G., Jiang, H., 2018. Broadband and ultrathin infrared stealth sheets. Adv. Eng. Mater. 20, 1800038. http://dx.doi.org/10.1002/adem.201800038.

Mohammadifar, M., Tahernia, M., Yang, JH., Koh, A., Choi, S., 2020. Biopower-on-skin: electricity generation from sweat-eating bacteria for self-powered e-skins. Nano Energy 75, 104994. http://dx.doi.org/10.1016/j.nanoen.2020.104994.

Nandakumar, DK., Ravi, SK., Zhang, Y., Guo, N., Zhang, C., Tan, SC., 2018. A super hygroscopic hydrogel for harnessing ambient humidity for energy conservation and harvesting. Energy Environ. Sci. 11, 2179–2187. http://dx.doi.org/10.1039/C8EE00902C.

Nandakumar, DK., Vaghasiya, JV., Yang, L., Zhang, Y., Tan, SC., 2020. A solar cell that breathes in moisture for energy generation. Nano Energy 68, 104263. http://dx.doi.org/10.1016/j.nanoen.2019.104263V.

Nandakumar, DK., Zhang, Y., Ravi, SK., Guo, N., Zhang, C., Tan, SC., 2019. Solar energy triggered clean water harvesting from humid air existing above sea surface enabled by a hydrogel with ultrahigh hygroscopicity. Adv. Mater. 31, 1806730. http://dx.doi.org/10.1002/adma.201806730.

Nozariasbmarz, A., Suareza, F., Dycus, JH., Cabralb, MJ., LeBeau, JM., Öztürk, MC., Vashaee, D., 2020. Thermoelectric generators for wearable body heat harvesting: Material and device concurrent optimization. Nano Energy 67, 104265. http://dx.doi.org/10.1016/j.nanoen.2019.104265.

Patchan, MW., Graham, JL., Xia, Z., Maranchi, JP., McCally, RL., Schein, OD., Elisseeff, JH., Trexler, MM., 2013. Synthesis and properties of regenerated cellulose-based hydrogels with high strength and transparency for potential use as an ocular bandage. Mater. Sci. Eng. C 33, 3069–3076. http://dx.doi.org/10.1016/j.msec.2013.03.037.

Peng, Y., Cui, Y., 2020. Advanced textiles for personal thermal management and energy. Joule 4, 724–742. http://dx.doi.org/10.1016/j.joule.2020.02.011.

Shi, Z., Gao, H., Feng, J., Ding, B., Cao, X., Kuga, S., Wang, Y., Zhang, L., Cai, J., 2014. In situ synthesis of robust conductive cellulose/polypyrrole composite aerogels and their potential application in nerve regeneration. Angew. Chem. Int. Ed. 53, 5380–5384. http://dx.doi.org/10.1002/anie.201402751.

Shrivastav, AM., Gunawardena, DS., Liu, Z., Tam, H., 2020. Microstructured optical fiber based Fabry-Pérot interferometer as a humidity sensor utilizing chitosan polymeric matrix for breath monitoring. Sci. Rep. 10, 6002. http://dx.doi.org/10.1038/s41598-020-62887-y.

Thomas, S., 2020. Electronic skins sweat it out. Nat. Electron. 3, 235. http://dx.doi.org/10.1038/s41928-020-0420-1.

Tong, R., Chen, G., Pan, D., Qi, H., Li, R., Tian, J., Lu, F., He, M., 2019a. Highly stretchable and compressible cellulose ionic hydrogels for flexible strain sensors. Biomacromolecules 20, 2096–2104. http://dx.doi.org/10.1021/acs.biomac.9b00322.

Tong, R., Chen, G., Pan, D., Tian, J., Qi, H., Li, R., Lu, F., 2019b. Ultrastretchable and antifreezing double-cross-linked cellulose ionic hydrogels with high strain sensitivity under a broad range of temperature. ACS Sustain. Chem. Eng. 7, 14256–14265. http://dx.doi.org/10.1021/acssuschemeng.9b03555.

Wang, Y., Dai, M., Wu, H., Xu, L., Zhang, T., Chen, W., Wang, ZL., Yang, Y., 2021. Moisture induced electricity for self-powered microrobots. Nano Energy 90, 106499. http://dx.doi.org/10.1016/j.nanoen.2021.106499.

Wei, S., Yin, R., Tang, T., Wu, Y., Liu, Y., Wang, P., Wang, K., Mei, M., Zou, R., Duan, X., 2019. Gas-permeable, irritation-free, transparent hydrogel contact lens devices with metal-coated nanofiber mesh for eye interfacing. ACS Nano 13, 7920–7929. http://dx.doi.org/10.1021/acsnano.9b02305.

Wu, C., Geng, H., Tan, S., Lv, J., Wang, H., He, Z., Wang, J., 2020. Highly efficient solar anti-icing/deicing via a hierarchical structured surface. Mater. Horiz. 7, 2097–2104. http://dx.doi.org/10.1039/D0MH00636J.

Yang, JC., Mun, J., Kwon, SY., Park, S., Bao, Z., Park, S., 2019. Electronic skin: recent progress and future prospects for skin-attachable devices for health monitoring, robotics, and prosthetics. Adv. Mater. 31, 1904765. http://dx.doi.org/10.1002/adma.201904765.

Yang, J., Zhang, X., Qu, H., Yu, ZG., Zhang, Y., Eey, TJ., Zhang, Y-W., Tan, SC., 2020. Adsorption-based atmospheric water harvesting device for arid climates. Adv. Mater. 32, 2002936. http://dx.doi.org/10.1038/s41467-018-03162-7.

Ye, D., Chang, C., Zhang, L., 2019a. High-strength and tough cellulose hydrogels chemically dual cross-linked by using low-and high-molecular-weight cross-linkers. Biomacromolecules 20, 1989–1995. http://dx.doi.org/10.1021/acs.biomac.9b00204.

Ye, D., Lei, X., Li, T., Cheng, Q., Chang, C., Hu, L., Zhang, L., 2019b. Ultrahigh tough, super clear, and highly anisotropic nanofiber-structured regenerated cellulose films. ACS Nano 13, 4843–4853. http://dx.doi.org/10.1021/acsnano.9b02081.

Yi, H., Lee, S., Ko, H., Lee, D., Bae, W., Kim, T., Hwang, DS., Jeong, HE., 2019. Ultra-adaptable and wearable photonic skin based on a shape-memory, responsive cellulose derivative. Adv. Funct. Mater. 29, 1902720. http://dx.doi.org/10.1002/adfm.201902720.

Ying, B., Chen, RZ., Zuo, R., Li, J., X., Liu, 2021. An anti-freezing, ambient-stable and highly stretchable ionic skin with strong surface adhesion for wearable sensing and soft robotics. Adv. Funct. Mater. 31, 2104665. http://dx.doi.org/10.1002/adfm.202104665.

Zhang, X., Ma, X., Hou, T., Guo, K., Yin, J., Wang, Z., Shu, L., He, M., Yao, J., 2019. Inorganic salts induce thermally reversible and anti-freezing cellulose hydrogels. Angew. Chem. Int. Ed. 58, 7366–7370. http://dx.doi.org/10.1002/anie.201902578.

Zhang, Y., Nandakumar, DK., Tan, SC., 2020a. Digestion of ambient humidity for energy generation. Joule 4, 2532–2536. http://dx.doi.org/10.1016/j.joule.2020.10.003.

Zhang, X., Yang, J., Borayek, R., Qu, H., Nandakumar, DK., Zhang, Q., Ding, J., Tan, SC., 2020b. Super-hygroscopic film for wearables with dual functions of expediting sweat evaporation and energy harvesting. Nano Energy 75, 104873. http://dx.doi.org/10.1016/j.nanoen.2020.104873.

Zhou, T., Wang, J., Huang, M., An, R., Tan, H., Wei, H., Chen, Z., Wang, X., Liu, X., Wang, F., He, J., 2019. Breathable nanowood biofilms as guiding layer for green on-skin electronics. Small 15, 1901079. http://dx.doi.org/10.1002/smll.201901079.

Zhu, M., Yi, Z., Yang, B., Lee, C., 2021. Making use of nanoenergy from human-nanogenerator and self-powered sensor enabled sustainable wireless IoT sensory systems. Nano Today 36, 101016. http://dx.doi.org/10.1016/j.nantod.2020.101016.